Rapid Load Testing on piles instrumented with glass fibre optics in Rotterdam

Rob van Dorp[i)], Rutger Buitenhuis[ii)] and Harm Kortmann[iii)]

i) Managing partner, Allnamics Geotechnical Experts BV, Den Haag, The Netherlands

ii) MSc student, Delft University of Technology, Delft, The Netherlands

iii) Project manager, Port of Rotterdam Authority, Rotterdam, The Netherlands

ABSTRACT

In Rotterdam Harbour a series of Rapid Load Tests (RLT) has been executed on precast concrete piles that were instrumented with optical fibres (FBG). The same piles had been subjected to Static Load Tests (SLT) a couple of weeks earlier. The results of these static load tests were presented and discussed at the ECSMGE conference in Reykjavik in 2019 [2]. The Rapid Load Tests have been performed in order to (a) test feasibility of fibre optics for capturing strain data at the high sample rate required for Rapid Load Testing, (b) use the opportunity to be able to distinguish the contributions of toe resistance and shaft friction (per layer) during a Rapid Load Test and (c) check and establish the correlation between results of Rapid Load Testing and Static Load Testing, including a break down between the soil layers contributing to toe resistance (only sand) and the soil layers contributing to shaft friction (dominated by stiff clay).

In international codes and guidelines, the correlation between Rapid Load Testing and static pile behaviour is accounted for by applying the so-called loading rate factor on the results. For piles in rock and granular soils this loading rate factor is pretty well known, but for piles in cohesive soils this correlation is less conclusive and subject to a larger variation. This paper discusses the comparison of results of RLT and SLT and the soil dependent loading rate factor that could be derived from the tests.

Keywords: Rapid Load testing, case history, loading rate factor, correlation Static Load Testing

1 INTRODUCTION

The new version of Dutch national pile design code NEN-EN_1997-1 became active in 2017. This included a reduction of default values for pile design factors. This reduction can be avoided by performing project based pile load tests that can confirm that less conservative design factors are allowed for the project. For this reason, a full-scale study was performed, comprising in-situ load tests at the Kramer Terminal in the Port of Rotterdam. The test campaign started with full-scale static load tests (SLT) conducted on prefabricated concrete piles. These piles were instrumented with fibre optic sensors (FBG) to perform strain measurements along the pile axis at multiple levels. This enabled separation of the contributions of shaft friction and toe resistance to total pile capacity

After completion of the static load tests, a series of rapid load tests (RLT) were conducted on the same piles using a Stat*Rapid* device. The objective was to compare the RLT results to the SLT results in terms of loading rate factors for shaft and toe.

The RLT results were elaborated using the unloading point method (UPM) as first proposed by Middendorp et al in 1992 [6].and later by Hölscher et al. in 2012 [4]. Part of the UPM is application of a loading rate factor (η or LRF) on the measured force in order to correct for the loading rate effect, which makes the pile and subsoil act stiffer when load is applied at a fast rate. The loading rate effect is not the same as damping and should therefore not be mixed up with it.

The applicable value of the loading rate factor depends on the soil type: for piles in granular soils and rock a higher loading rate factor (i.e. smaller correction) has to be used than for piles in cohesive soils. Next to that, the loading rate factor in cohesive soils (like clay) have a wider range of variation, depending on various soil properties. From a large number of correlation tests, the loading rate factor for sand is established at $\eta = 0.94$ with a coefficient of variation of 0.15 [4]. For cohesive soils the loading rate factor is

established at η = 0.66 with a coefficient of variation of 0.49 [4]. These average values are also mentioned in ISO 22477-10:2016.

By means of derived force along the pile axis, obtained with strain monitoring with the FBG's, it is possible to set up load-displacement diagrams for both the full pile and the pile toe, for both SLT and RLT. From these diagrams the corresponding loading rate factors can be derived for shaft and toe, for all piles.

2 SOIL CONDITIONS

Prior to the installation of the test piles several CPT's had been executed in order to investigate the geotechnical properties of the soil at the test location in the Port of Rotterdam. The soil classification is based on SBT charts as proposed by Robertson [1]. The soil profile is shown in Fig. 1. The dashed lines indicate the interfaces between the different relevant soil layers penetrated by the pile. The pile toe is situated at NAP -32.0 m, which is approx. 0.5 m into layer 7 in fig. 1.

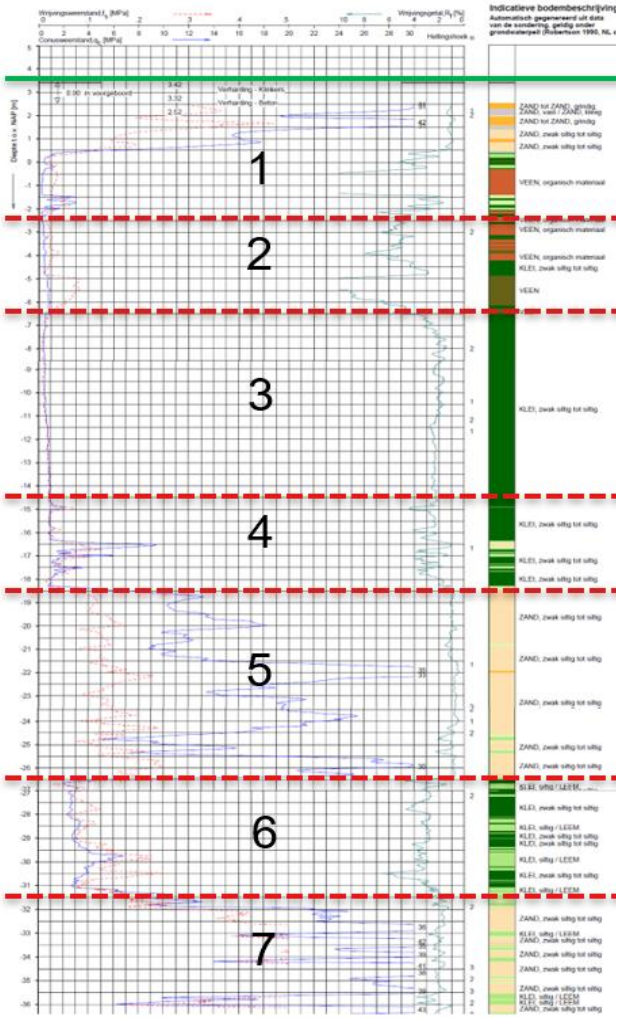

Fig. 1: Soil profile at test location.

The soil profile is divided into 7 relevant main layers, see fig. 1 and table 1 below.

Table 1: Soil profile

Layer	Depth (NAP)	Soil Type
1	+3.3 to -2.5	Sand (fill)
2	-2.5 to 6.5	Peat
3	-6.5 to -14.5	Soft clay
4	-14.5 to -18.5	Medium Clay with sand
5	-18.5 to -26.5	Medium Sand
6	-26.5 to -31.55	Stiff clay
7	-31.55 to -40	Dense sand

With the pile toe penetration being only 0.5 m into sand layer 7, the behaviour of the pile in terms of loading rate effect is highly dominated by the clay layers around the shaft. This implied that an overall loading rate factor η = approx. 0.6 or lower could be expected. This translates to considerable higher RLT test loads to bring the piles to full geotechnical failure.

3 RESULTS STATIC LOAD TEST

3.1 General setup

Referral is made to reference [2] for more elaborate presentation and discussion of the SLT results, in which the authors were not involved. Three out of four piles exhibited geotechnical failure during SLT and are therefore presented in [2] and considered here in the comparison with RLT. The piles are 450 x 450 mm and 36 meters in length..

Fig. 2: Static Load Test [2].

All the piles were instrumented with optical fibres (FBG), attached to the reinforcement at 23 predefined levels in the pile along the entire length of the piles. The uppermost strain measurement was taken at NAP -2.5 m (6.6 m below pile head). and the lowest at NAP -31.55 m which is 0.45 m above pile toe.

3.2 Elaboration

The measured strains at each level in the pile are translated to corresponding normal forces according to Hooke's law:

$$F = EA\varepsilon \qquad (1)$$

In which F is the normal force (kN), EA is the axial stiffness (kN) and ε the strain (-) in the pile, measured by the FBG. Determination of the correct axial stiffness of each pile is crucial for elaboration. In the SLT report [2],

the strain dependent axial stiffness EA was established for each pile according to Fellenius' approach (2001) [7]. For increasing strains the relation between strain and stiffness gradually becomes linear, see Fig. 3.

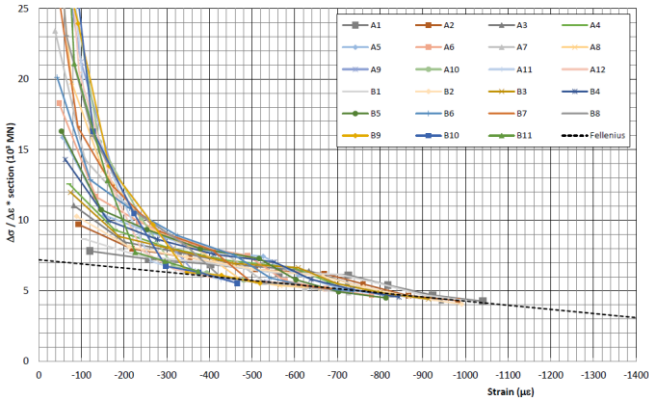

Fig. 3: Strain dependent axial stiffness EA according to Fellenius for Pile 1 [2].

Using the strain dependent axial stiffness EA and the measured strains at different levels in the pile, the associated force distribution along the pile axis was generated for each load step of the SLT, see example for pile 1 in figure 4. The curves from left to right represent the consecutive (increasing) load steps, in this case with a maximum force of 6,407 kN at pile head level and 2,511 kN at pile toe level.

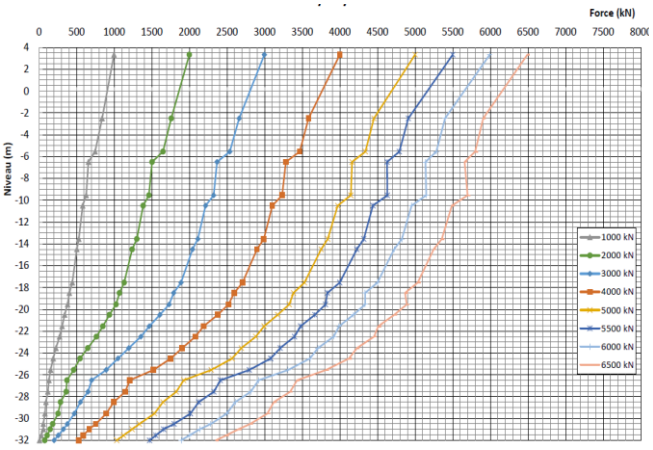

Fig. 4: Force distribution along Pile 1 during SLT [2].

The established normal force at the level of the lowest sensor at NAP -31.55 m (0.45 m above pile toe level) is considered pile toe resistance. The difference in axial force between the uppermost sensor and lowest sensor is assigned to the total pile shaft friction.

3.2 Results

In figure 5 the load displacement curves for pile head, pile toe and pile shaft are displayed in one combined graph for all piles. This makes the graph a bit hard to read; important here are the left cluster (pile toe) and right cluster (full pile). The 3 test piles show pretty consistent behaviour, with the maximum mobilized toe capacity ranging between approx. 2,000 kN and 2,500 kN and the mobilized total capacity between approx. 6,400 kN and 6,700 kN. In accordance with Eurocode and [3] pile capacity was established as the pile load at the moment that the (maximum) displacement of the pile toe had reached 10% of the equivalent pile diameter, which is 51 mm in this case. For pile 1 this included some extrapolation of the measured curve.

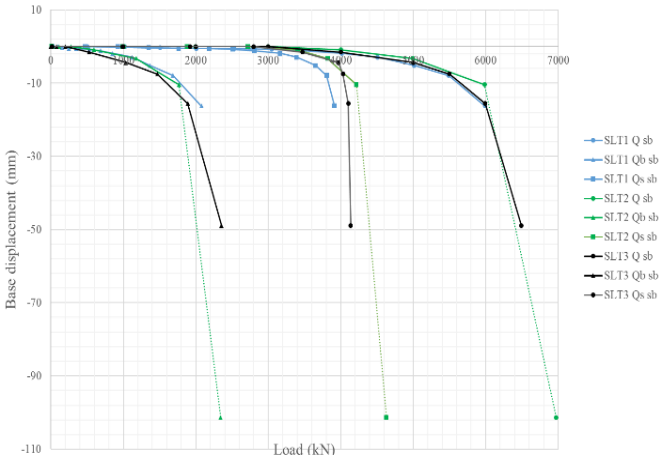

Fig. 5: Load-displacement diagrams SLT [2].

Table 2 below provides an overview of the established ultimate bearing capacities of full pile, pile toe and pile shaft for all 3 piles.

Table 2: Pile capacity for SLT, differentiated to shaft capacity and toe capacity

Pile	R_{pile} $[kN]$	R_{base} $[kN]$	R_{shaft} $[kN]$
1	6,407	2,511	3,896
2	6,610	2,418	4,192
3	6,706	2,063	4,643

4 RAPID LOAD TEST

4.1 Stat*Rapi*d device

The principle of StatRapid concerns dropping a drop mass on a spring assembly, placed in-between the pile head and the drop mass. The spring assembly lenghtens the duration of the blow such, that the pile will behave quasi static. Consequently (in deviation from Dynamic Load Testing) complex wave patterns do not need to be assessed for elaboration and interpretation of RLT.

Fig. 6: Rapid Load Test (StatRapid).

The required drop mass is approximately approx. 5% of the required mobilized static capacity. During each load cycle the force exerted on the pile head is recorded, as well as the displacement and acceleration of the pile head. From the recorded data the stiffness of the pile, the load-displacement behaviour of the pile and the maximum mobilised capacity can be determined. The StatRapid device has a built-in hydraulic lift, with which the exact drop height can be set. Subsequently the drop mass is hydraulically released and after the drop mass has bounced back from the pile head for the first time, a hydraulic catching mechanism secures the drop mass at its highest position. Consequently a second blow on the pile head is avoided, making it possible to perform multi-cycle testing with cycles increasing in magnitude.

4.1 Unloading Point Method (UPM)

The Unloading Point Method (UPM, [6]) is used to calculate the mobilized static pile resistance [4]. Application of the UPM is visualized in figure 7. The graphs concern (from top to bottom) measured force, displacement, velocity and acceleration vs. time during a single load cycle. The red dotted line is the time of the unloading point.

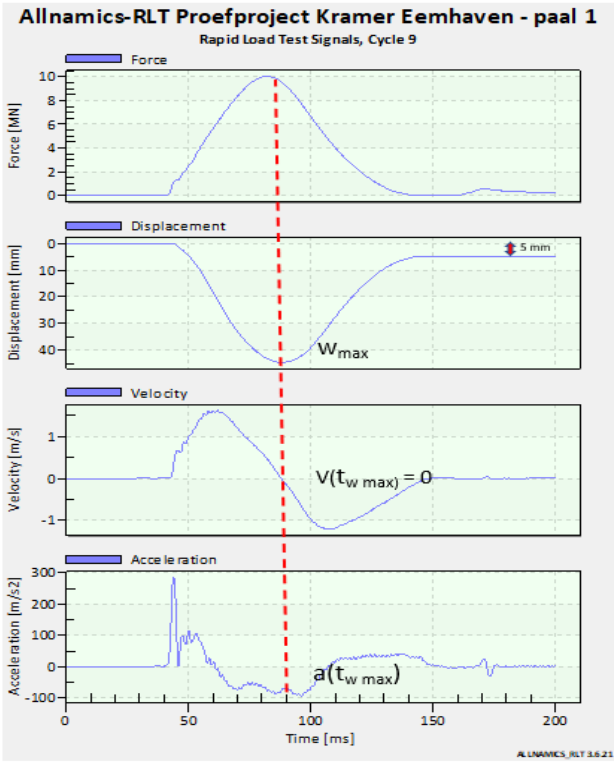

Fig. 7: Visualization of the UPM,. Measured force, displacement, velocity and acceleration vs. time during a load cycle. red dotted line is unloading point.

At the point of unloading, the pile velocity is zero. As a consequence the damping force is zero, so the only acting forces balancing each other are the applied rapid load force, the mobilized static soil resistance and the inertia force. These are all known. The mobilized resistance of the pile during a RLT is obtained by correcting the rapid load on the pile head for pile mass inertia at the point of unloading, i.e., maximum displacement ($t = t_{w,max}$).

$$F_{soil}(t) = F(t) - F_{inertia}(t) = F(t) - m \cdot a(t) \quad (2)$$

The measured forces and pile head displacements can be plotted against each other for each load cycle, resulting in a rapid load displacement diagram. See figure 8.

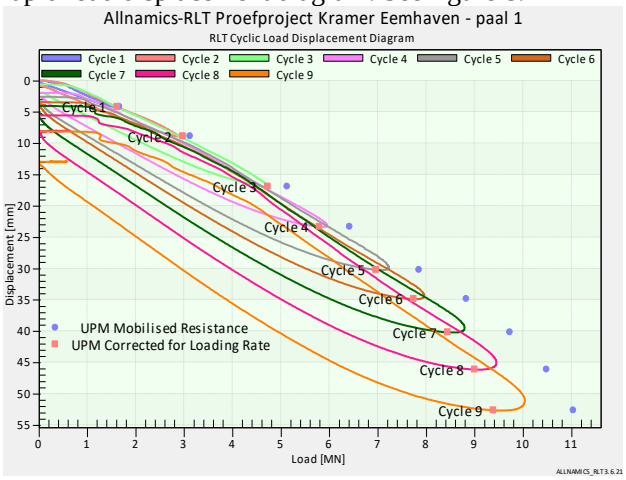

Fig. 8: multiple load cycles rapid load displacement diagram (using standard overall loading rate factor η = 0,94)

Once the rapid load is corrected for inertia effects a loading rate factor (η) needs to be applied to the force to account for the loading rate effect, which makes the pile and subsoil act stiffer when load is applied at a fast rate. In general, the soil resistance at the unloading point, after correction for inertia and loading rate effect, is a point on the static load-displacement curve.

$$F_{stat,der}(t_{w\,max}) = \eta[F(t_{w\,max}) - m \cdot a(t_{w\,max})] \quad (3)$$

Applicable values for the loading rate factor have been discussed earlier in this paper.

4.2 Separation of toe and shaft from measured strains

As mentioned earlier, the FBG's in the test piles were monitored during each load cycle. See figure 9, showing the measured strains vs. time at all monitoring levels during a single load cycle.

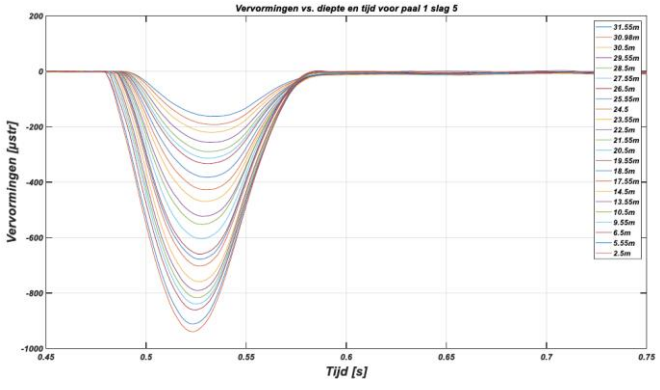

Fig. 9: measured strains embedded FBG's during RLT load cycle

The measured strains have been translated to corresponding normal forces in the pile, using the same strain dependent pile stiffness EA as for the SLT. This made it possible to establish distribution of normal force vs. depth during each load cycle

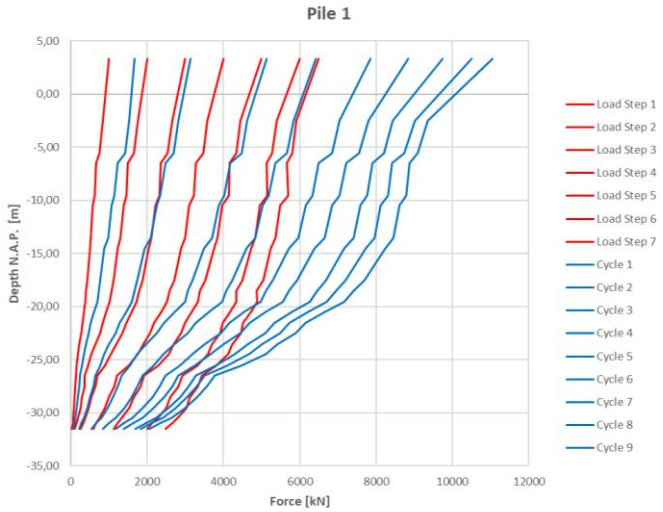

Fig. 10: Force distribution over depth for pile 1 during SLT and RLT.

Fig. 10 shows a comparison between the axial force distribution for respectively each SLT load step (in red) and each RLT loading cycle (in blue), for test pile 1, without application of an LRF. The outermost right red curve concerns the highest SLT load step (at ultimate capacity); the outermost right blue curve concerns the highest RLT load step.

The established mobilized pile capacity, and its division over shaft and toe, at the unloading point of the maximum load cycle, based on η = 0,94, are shown for the 3 test piles in Table 3.

Table 3: Maximum mobilized pile capacity divided into pile shaft and toe resistance for RLT, using η = 0,94

Pile	R_{pile} [kN]	R_{base} [kN]	R_{shaft} [kN]
1	12,521	2,740	9,781
2	11,490	2,443	9,047
3	10,833	2,441	8,392

The graphs in figure 10 are a bit hard to read; important here are the following observations:

1. At pile head level the maximum RLT load ranged between 10.8 and 12.5 MN, without reaching full geotechnical failure of the piles. The ratio between capacity established with SLT and the maximum RLT load ranges between 0.51 and 0.62. This indicates that the applicable overall LRF has to be considerably lower than the standard value of η =0,94 for piles in sand. This confirms that the loading rate behaviour of the pile is indeed highly influenced by the clay layers around the shaft.
2. At pile toe level the maximum RLT load ranged between 2.44 and 2.74 MN. The ratio between pile toe capacity established with SLT and the maximum RLT load at pile toe level ranges between 0.85 and 0.99. Because the pile toe is driven into sand, this indicates that the standard value of η =0,94 for piles in sand is confirmed by this test.
3. The soil around the pile shaft is dominated by (stiff) clay, for which loading rate factors in the range of η = 0,40 – 0,66 can be expected. In combination with the indicated LRF for the pile toe (η = 0,94) this seems consistent with the indicated overall LRF for the full pile in the first observation.

4.3 Rollberg extrapolation

In order to compare the results from RLT with SLT in terms of a loading rate factor (η), the load-displacement curves for both tests are needed for every pile. As already mentioned, the SLT brought all the 3 piles to geotechnical failure, but due to the significant loading rate effects of the shaft during RLT, none of the piles was brought to complete geotechnical failure during RLT. See example in figure 11 below; showing only a start of geotechnical failure at the last load cycle.

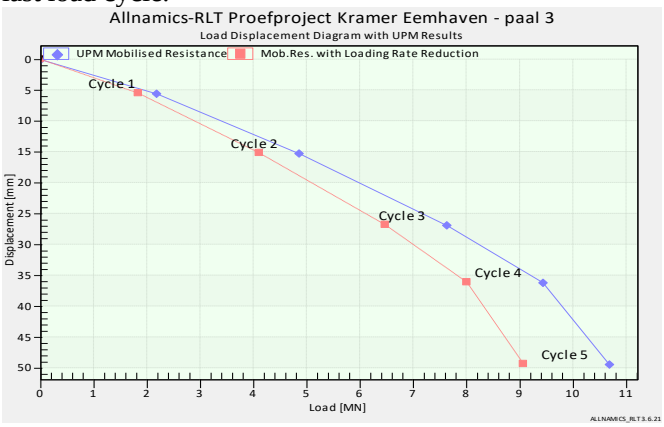

Fig. 11: RLT load-displacement diagram pile 3

Consequently, it was necessary to extrapolate the measured load-displacement curve beyond the last measurement load step, in order to establish the ultimate capacity for RLT.

Extrapolation is done following the method proposed by Rollberg [5]. This method uses a mathematical equation to define a hyperbolic load-displacement curve. The method has the ability to extrapolate the load-displacement curve beyond the maximum test load to the plunging limit. The hyperbolic equation is presented in Equation 4.

$$Q(s) = \frac{s}{a + b \cdot s} \qquad (4)$$

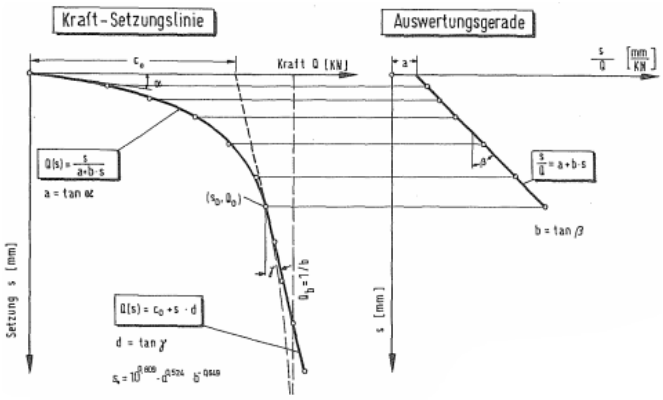

Fig. 12: Rollberg extrapolation method [5]

The parameters to derive the hyperbolic function are a and b. They respectively represent the offset at zero displacement and the slope of the regression line in the s/Q vs. s diagram (right plot in Fig. 12). In a load-displacement curve a and b represent respectively the initial stiffness and ultimate soil resistance at failure.

The best linear line fit through the measurement points in the s/Q vs s diagram is established by linear regression. For this, multiple linear regression lines have been made by selecting different sets of data points and excluding outliers. Each set of a specific set of datapoints is one permutation. In

a linear regression line for a single permutation is visualized. The points selected for the permutation shown in the graph are encircled.

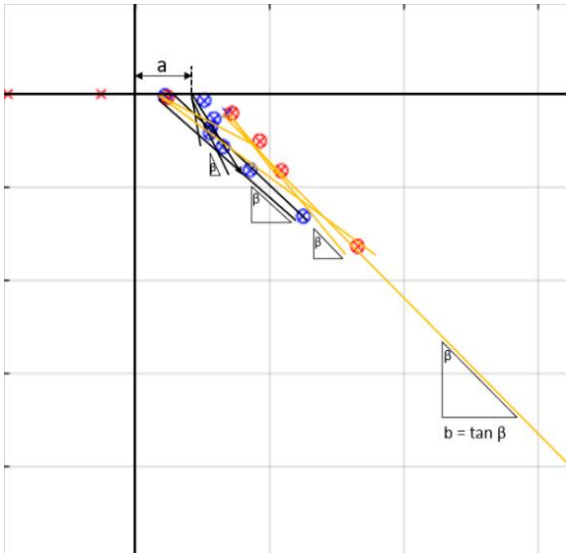

Fig. 13: Visualization of parameters a and b for a linear regression line for SLT (red) and RLT (blue).

Based on the offset and inclination of each regression line for each permutation a value for a and b is calculated. After completion of all (permutations of the) linear regressions a histogram for all calculated values of parameters a and b is made to find the median values for both. For each pile, the median values of a and b are used in the hyperbolic load-displacement curve according to Rollberg's method. The result is presented and discussed in the next chapter.

4.4 SLT & RLT load-displacement graphs compared

Figure 14 shows the maximum displacement and corresponding forces at pile *head* level toe for both SLT and extrapolated RLT (derived using the Rollberg method as discussed above) for all the 3 piles. The left cluster are the SLT results; the right cluster the RLT results. The overall differences are as observed in chapter 4.2.

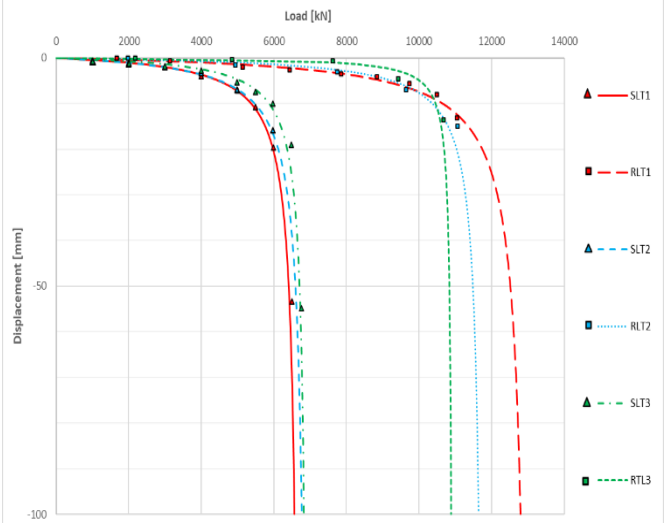

Fig. 12: Load-displacement diagrams at pile head level for SLT & RLT. SLT graph measured, RLT graph extrapolated.

Figure 15 shows the maximum displacement and corresponding forces at pile *toe* level toe for both SLT

and extrapolated RLT (derived using the Rollberg method as discussed above) for all the 3 piles. In this graph the RLT results are consistent with the SLT results, as also observed in chapter 4.2. Furthermore it can be seen that the hyperbolic functions established with Rollberg's method using linear regression properly represent the data points of the load-displacement diagrams for both SLT and RLT. The same applies for figure 14.

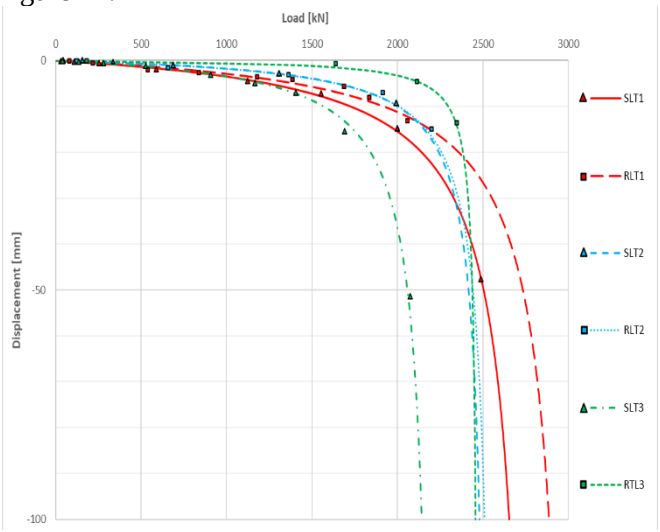

Fig. 13: Load-displacement diagram for the pile toe SLT measured, RLT extrapolated.

For pile 2 (blue short dashed and round dotted lines) in figure 15 it can be seen that there are hardly any loading rate effects visible at the pile toe. For the other piles a difference in toe resistance between SLT and RLT is visible. The differences are 8% (pile 1, red solid and long dashed lines) and 15% (pile 3, short dashed-dotted and green square dotted lines). For piles 1 and 2 the difference between RLT and SLT is consistent with the known loading rate factor for sand (η = 0,94 = difference 6%); for pile 3 the difference is a bit larger. A possible explanation for this might be that pile 3 has less or no penetration into the deep sand layer (see fig. 1, layer 7), increasing the influence of the clay around the shaft on the overall loading rate effect. This is supported by the shapes of the load-displacement curves in fig. 15: piles 1 and 2 show a similar response for both SLT and RLT, whereas pile 3 initially acts stiffer for RLT compared to SLT, followed by a plunging failure type.

4.5 Loading Rate Factors

Loading rate factors (LRF or η) are used to correct the value for the mobilized static resistance obtained by the rapid load test to the long term static resistance due to loading rate effects.

$$\eta = \frac{R_{stat,SLT}}{R_{stat,der\ RLT}} \qquad (5)$$

LRF can be obtained by using the calculated soil resistance at geotechnical failure for both the SLT and the extrapolated curve from the RLT, at maximum pile toe displacement 0,1*D_{eq} = 0,51 mm. The overall LRF can be subdivided into separate LRF's for pile shaft and pile toe resistance:

$$\eta = x_{toe} \cdot \eta_{toe} + x_{shaft} \cdot \eta_{shaft} \qquad (6)$$

With x_{toe} and x_{shaft} the relative contributions (in %) of shaft and toe to the total pile capacity. In this case, values for both can be derived from table 2 and table 3 for SLT and RLT respectively.

Table 4: relative contributions (%) of shaft and toe resistance to mobilized total capacity per testpile.

Test	**Pile**	x_{toe} **[%] sand**	x_{shaft} **[%] clay**
SLT	1	39	61
	2	37	63
	3	31	69
RLT	1	22	78
	2	21	79
	3	23	77

The overall LRF for a RLT is derived in Equation (7)

$$\eta = \frac{R_{toe}}{R_{pile}} \cdot \eta_{toe} + \frac{R_{shaft}}{R_{pile}} \cdot \eta_{shaft} \qquad (7)$$

The LRF for only the pile toe is relatively easy to determine by means of comparing the pile toe resistance at failure for both SLT and RLT, for the lowest sensor level (NAP -31.5 m).

$$\eta_{toe} = \frac{R_{toe\ SLT}}{R_{toe,der\ RLT}} \qquad (8)$$

The LRF for the pile shaft is a combination of all the individual layers and taken as one equivalent overall shaft LRF using .

Table 4 and Table 3.

$$\eta_{shaft} = \frac{R_{shaft\ SLT}}{R_{shaft,der\ RLT}} \qquad (9)$$

In table 5 the overall values and differentiated LRF values are further outlined for all the piles

Table 5: Overall Loading Rate Factors and differentiated loading rate factors (toe & shaft) for each pile

Pile	$\eta_{overall}$ **[-]**	η_{toe} **[-] sand**	η_{shaft} **[-] clay**
1	0.51	0.92	0.39
2	0.58	0.99	0.46
3	0.62	0.85	0.55

Table 5 confirms the loading rate effect of the clay layers around the shaft has a large influence on the overall LRF for the pile.

Table 5 also confirms the recommended value $\eta = 0.94$ (with variation coefficient 0.15) for the pile toe, which is driven into sand.

5 CONCLUSIONS

In the Port of Rotterdam, a series of Rapid Load Tests (RLT) was executed on instrumented prefab concrete piles, using a Stat*Rapid* device. The piles were previously tested by Static Load Testing (SLT) a few weeks earlier. This paper presented the results of a study comparing the mobilized capacity from the static load tests to the derived mobilized static capacity from the rapid load tests.

The paper quantifies the experienced loading rate effects for all piles by differentiating the contributions of pile shaft and pile toe. Significant loading rate effects around the shaft were observed during RLT, which resulted in none of the piles reaching geotechnical failure, even though the loads exerted on the pile head were larger than during the SLT's.

Consequently, the load displacement curves for the RLT had to be extrapolated to establish ultimate resistance during RLT. This was done by means of the Rollberg method [5], which uses a hyperbolic function to describe the relationship between the load and the maximum displacement of each pile.

Based on these extrapolated load displacement diagrams, made for the full pile and for the pile toe only, loading rate factors were attributed to every pile for rapid loading. This included differentiation between loading rate factors for the shaft (dominated by clay layers) and the pile toe (driven into sand).

For the pile toe, situated in sand, the LRF ranges from 0.85 to 0.99. This is very well in line with the value for LRF for piles in sand ($\eta = 0{,}94$) as recommended in [4] and ISO 22477-10:2016. For the pile shaft, dominated by stiff clay layers, the LRF's range from 0.39 to 0.55. This is consistent with the average value and (large) variation range for clay mentioned in [4].

Because of the low values for the LRF for the shaft (dominated by clay layers), the resulting overall value for the whole pile ranges from 0.51 to 0.61. This demonstrates that, for piles with the shaft in cohesive soils and the toe in sand, it is important to take the influence of the cohesive layers on shaft friction behavior in account when preparing a Rapid Load Test or when elaborating and interpreting the results.

Although the soil around the shaft does not only contain clay layers, but also sand layers, the results of the elaboration of RLT indicate that the deepest cohesive layer within the penetration depth of the pile is decisive for the loading rate behavior of all soil layers encountered above that layer.

6 REFERENCES

[1] P. Robertson, "Interpretation of cone penetration tests a unified approach," Canadian Geotechnical Journal, 2009.

[2] I. Matic, R. de Nijs, M. de Vos and A. Roubos, "Full-scale load testing on long prefabricated concrete piles in the Port of Rotterdam," in *XVII European Conference ECSMGE-2019 Reykjavik on Soil Mechanics and Geotechnical Engineering*, 2019.

[3] R. Frank, C. Bauduin, R. Driscoll, M. Kavvadas, N. Krebs Ovesen, T. Orr and B. Schuppener, "Designers' Guide to EN 1997-1 Eurocode 7: Geotechnical Design – General Rules," ICE Publishing, 2015.

[4] P. Holscher, H. Brassinga, M. Brown, P. Middendorp, M. Profittlich and F. van Tol, "Rapid Load Testing on Piles: Intepretation Guidelines (CUR publication 230)," 2012.

[5] D. Rollberg, "Die Kraft-Setzunglinie von Pfalen," Bauingenieur, vol. 53, pp. 309-313, 1978.

[6] Middendorp, P., Bermingham, P., Kuiper B., 1992. Statnamic testing of foundation piles. 4th International Conference on Stress Waves, The Hague, Balkema

[7] Fellenius, B. H., 2001. From Strain Measure-ments to Load in an Instrumented Pile, Geotechnical News Magazine.